Doppler Compensation & Single Pulse Imaging using Adaptive Pulse Compression

SHANNON D. BLUNT, Senior Member, IEEE
University of Kansas

AARON K. SHACKELFORD, Member, IEEE

KARL GERLACH, Fellow, IEEE
U.S. Naval Research Laboratory

KEVIN J. SMITH
University of Kansas

The effects of target Doppler are addressed in relation to adaptive receive processing for radar pulse compression. To correct for Doppler-induced filter mismatch over a single pulse, the Doppler-compensated adaptive pulse compression (DC-APC) algorithm is presented whereby the respective Doppler shifts for large target returns are jointly estimated with the illuminated range profile and subsequently incorporated into the original APC adaptive receive filter formulation. As a result, the Doppler-mismatch-induced range sidelobes can be suppressed thereby regaining a significant portion of the sensitivity improvement that is possible when applying adaptive pulse compression (APC) without the existence of significant Doppler mismatch. In contrast, instead of compensating for Doppler mismatch, the single pulse imaging (SPI) algorithm generalizes the APC formulation for a bank of Doppler-shifted matched filters thereby producing a sidelobe-suppressed range-Doppler image from the return signal of a single radar pulse which is applicable for targets with substantial variation in Doppler. Both techniques are based on the recently proposed APC algorithm and its generalization, the multistatic adaptive pulse compression (MAPC) algorithm, which have been shown to be effective for the suppression of pulse compression range sidelobes thus dramatically increasing the sensitivity of pulse compression radar.

Manuscript received April 20, 2007; revised February 5, 2008; released for publication April 20, 2008.

IEEE Log No. T-AES/45/2/933011.

Refereeing of this contribution was handled by A. Lanterman.

This work was supported by the United States Office of Naval Research ONR 31.

Authors' addresses: S. D. Blunt and K. J. Smith, Dept. of Electrical Engineering & Computer Science, University of Kansas, 1520 W. 15th St., Eaton Hall, Rm 3034, Lawrence, KS 66045, E-mail: (sdblunt@eecs.ku.edu); A. K. Shackelford and K. Gerlach, Radar Division, Naval Research Laboratory, Washington, D.C.

I. INTRODUCTION

Pulse compression is commonly used in radar as a means to allow for the transmission of a long pulse, thereby illuminating a target with adequate energy for detection, while maintaining the range resolution of a short duration pulse through phase or frequency modulation of the pulse. It is well known [1] that for a solitary point scatterer in white Gaussian noise the signal-to-noise ratio (SNR) of the pulse compressed output is maximized through the use of a filter matched to the transmitted waveform (i.e., the modulated long pulse). As such, the matched filter thereby maximizes the detectability of the solitary scatterer in noise. However, in the presence of multiple scatterers, the matched filter is suboptimal due to range sidelobes induced by the matched filtering operation. The range sidelobes of a large scatterer can mask the presence of nearby smaller scatterers, thus limiting the sensitivity of the matched filter. The ability of the matched filter to extract a single target in the presence of other nearby targets is indicated by the autocorrelation (or in general the ambiguity surface) of the transmitted waveform scaled by the amplitudes of the nearby large targets. Hence, the performance of the matched filter in a dense scatterer environment is fundamentally limited due to masking caused by the nearby large targets. The target masking problem can be partially alleviated by using mismatched filters often based on least squares (LS) estimation [2–4], albeit at the cost of spreading the sidelobes over a greater range extent. Furthermore, mismatched filters (as with the matched filter) are deterministic and therefore are generally not capable of completely suppressing particular range sidelobes due to the fact that they must be designed to suppress all possible sources of sidelobe interference (albeit only partially as a result of finite design degrees-of-freedom).

In realistic environments, targets of interest are often in motion and it is often the Doppler phase shift induced by this relative motion between the radar and a target that can enable the detection of a target when it is in the presence of stationary background clutter. However, large Doppler shifts over the length of a single pulse (i.e., the radar waveform), which are caused by high relative target velocities and/or the use of long waveforms, can be quite detrimental to radar detection performance due to severe mismatch between the expected and actual received waveforms (even when using Doppler-tolerant waveforms such as linear FM [1] or various discrete polyphase codes [5–6]). The result of this mismatch is reduced target SNR as well as an overall increase in range sidelobe levels. In fact, a very high time-bandwidth product coupled with extraordinarily high target velocity can cause relativistic effects [7–9] whereby the reflected radar waveform undergoes dilation in time thus exacerbating the mismatch, though such extreme

effects are not considered here. It is well known that a bank of phase-shifted matched filters tuned to the expected target velocities can compensate for the SNR loss due to Doppler mismatch. However, this does nothing to address the inherent range sidelobes of the matched filter. For LS-based mismatched filters, the effects of large Doppler can be more severe since it is inherently more sensitive than matched filtering and because LS estimation is known to be nonrobust to deviations from the assumed signal model [10].

Recently, an adaptive approach based upon a recursive implementation of minimum mean-square error (MMSE) estimation known as adaptive pulse compression (APC) has been developed [11–13] which is capable of almost complete range sidelobe mitigation thereby enabling estimation of the range profile illuminated by a radar to the level of the noise. Furthermore, for solitary low SNR targets, it has been shown [13] that APC essentially converges to the matched filter thereby maximizing detectability of the target. As such, APC facilitates the detection of small targets even when masked by much larger nearby targets. The elimination of range sidelobes is accomplished by adaptively estimating the appropriate receiver pulse compression filter to use for each individual range cell according to the relative power estimates of the surrounding range cells. For a given range cell, the respective filter places nulls at the relative range offsets of nearby large scatterers, thus suppressing their sidelobes. Each adaptive filter is obtained via a bootstrapping operation with the standard matched filter being used to obtain the initial estimate of the range profile.

The APC approach has been shown [11–13] to be superior to both standard matched filtering and LS-based mismatched filtering. However, due to its increased sensitivity, the performance gain provided by APC is diminished whenever the return signals from large targets exhibit significant Doppler phase shifts. Since it is generally expected that the received return signal is comprised of delayed and attenuated versions of the transmitted waveform, a substantial Doppler shift induced by a moving target will result in a mismatch between the expected received signal and the actual received signal. Hence, the ability of APC to sufficiently null the sidelobe interference from a large target exhibiting a significant Doppler shift is thereby limited by the degree of the Doppler-induced mismatch.

In this paper, some particular aspects of Doppler processing are examined in order to account for Doppler-induced mismatch over a single pulse such that the APC formulation can be employed either to 1) compensate for Doppler mismatch and thus fully suppress range sidelobe interference or to 2) use the additional Doppler information to perform imaging of relatively high-speed targets (though not so high as to enter the relativistic regime). For the first technique, a new formulation of APC is developed in which the illuminated range profile is jointly estimated with the Doppler shifts of large target returns. As a result, the Doppler-compensated APC (DC-APC) algorithm is shown to suppress range sidelobes nearly to the level of the noise even when the range profile contains large, fast-moving targets (e.g. a Mach 2 target illuminated by a 1 μs pulse from an X-band radar) which induce a significant Doppler mismatch. The APC formulation is also applied as a means to obtain some imaging capability using only a single pulse. In essence, the single pulse imaging (SPI) algorithm models the received signal as the superposition of numerous Doppler-shifted versions of the transmitted signal such that a bank of Doppler-tuned adaptive filters can be applied to produce a sidelobe-suppressed range-Doppler image. The SPI algorithm is in fact a variant of the multistatic generalization of APC denoted as MAPC [14–16] and is shown to yield much greater visibility over the single pulse than could be obtained by using a bank of matched filters.

The remainder of the paper is organized as follows. In Section II a generalized signal model accounting for Doppler effects is presented along with a brief discussion of the APC algorithm. For the generalized signal model the resulting algorithms for DC-APC and SPI are then presented in Section III. Finally, the performance capability of DC-APC and SPI are illustrated in Section IV.

II. GENERALIZED SIGNAL MODEL AND APC

It is well known that matched filtering [1] maximizes the received SNR of a solitary point scatterer in additive white Gaussian noise (AWGN) by convolving the received return signal with a complex-conjugated time-reversed version of the transmitted waveform. In the discrete domain, matched filtering can be represented as

$$\hat{x}_{\mathrm{MF}}(l) = \mathbf{s}^{\mathrm{H}}\mathbf{y}(l) \tag{1}$$

where $\hat{x}_{\mathrm{MF}}(l)$ is the matched filter estimate of the lth delayed sample of a length-L section of the range profile impulse response for $l = 0, 1, \ldots, L-1$ (i.e., the processing window), the length-N vector $\mathbf{s} = [s_0 \;\; s_1 \cdots s_{N-1}]^{\mathrm{T}}$ represents the sampled version of the transmitted waveform, $\mathbf{y}(l) = [y(l) \;\; y(l+1) \cdots y(l+N-1)]^{\mathrm{T}}$ is a vector of N contiguous samples of the complex received signal, and $(\cdot)^{\mathrm{T}}$ and $(\cdot)^{\mathrm{H}}$ are the transpose and complex-conjugate transpose (or Hermitian) operations, respectively.

The signal reflected by a solitary scatterer can be modeled at the receiver (after conversion to baseband) as $y(t) = \alpha s(t-\tau)e^{j\omega_d(t-\tau)}$ where α is the complex amplitude, τ is some relative time delay, and ω_d is Doppler frequency (in radians). Discretizing this continuous model, generalizing to multiple possible

scatterers over the extent of the waveform, and including noise, each discrete sample of the received signal can, in general, be expressed as

$$y(l) = \tilde{\mathbf{x}}^{\mathrm{T}}(l)\mathbf{s} + v(l) \tag{2}$$

where $\tilde{\mathbf{x}}(l)$ is modeled as

$$\tilde{\mathbf{x}}(l) = \mathbf{x}(l) \circ \mathbf{e}(l) \tag{3}$$

in which $\mathbf{x}(l) = [x(l)\ \ x(l-1)\cdots x(l-N+1)]^{\mathrm{T}}$ is the vector of N contiguous samples of the range profile impulse response, $v(l)$ is additive noise, and $\circ$ indicates the Hadamard product (element-by-element multiplication). The N-dimensional vector $\mathbf{e}(l) = [1\ \ e^{j\theta_{l-1}}\cdots e^{j(N-1)\theta_{l-N+1}}]$ is the relative phase shifts of the N contiguous samples of $\mathbf{x}(l)$ where θ_l is the Doppler phase shift between successive received samples induced by target motion at the lth range cell. The collection of N contiguous samples of the received signal can therefore be expressed as the generalized signal model

$$\mathbf{y}(l) = \tilde{\mathbf{X}}^{\mathrm{T}}(l)\mathbf{s} + \mathbf{v}(l) \tag{4}$$

where $\mathbf{v}(l) = [v(l)\ \ v(l+1)\cdots v(l+N-1)]^{\mathrm{T}}$ and

$$\tilde{\mathbf{X}}(l) = \begin{bmatrix} x(l) & x(l+1) & \cdots & x(l+N-1) \\ x(l-1)e^{j\theta_{l-1}} & x(l)e^{j\theta_l} & \ddots & \vdots \\ \vdots & \ddots & \ddots & x(l+1)e^{j(N-2)\theta_{l+1}} \\ x(l-N+1)e^{j(N-1)\theta_{l-N+1}} & \cdots & x(l-1)e^{j(N-1)\theta_{l-1}} & x(l)e^{j(N-1)\theta_l} \end{bmatrix} \tag{5}$$

is a collection of N length-N sample-shifted snapshots (in the columns) of the Doppler phase-shifted range profile impulse response. For pulse compression, the term on the main diagonal of (5) contains the desired information to be estimated while the off-diagonal terms effectively act as interference. It is this generalized signal model from which the DC-APC and the SPI algorithms are derived.

The original APC algorithm [7–9] did not exploit Doppler information and can thus be obtained from (4) and (5) by setting $\theta_{l-N+1} = \cdots = \theta_{l+N-1} = 0$ (or $\mathbf{e}(l) = \mathbf{1}$). For the lth range cell, the APC algorithm operates by replacing the matched filter $\mathbf{s}$ in (1) with the $N \times 1$ adaptive MMSE filter $\mathbf{w}(l)$ which is found to be [13]

$$\mathbf{w}(l) = \rho(l)(\mathbf{C}(l) + \mathbf{R})^{-1}\mathbf{s}. \tag{6}$$

The term $\rho(l) = |x(l)|^2$ is the power of the lth range cell, $\mathbf{R}$ is the $N \times N$ noise covariance matrix, and the signal correlation matrix $\mathbf{C}(l)$ is given by

$$\mathbf{C}(l) = \sum_{n=-N+1}^{N-1} \rho(l+n)\mathbf{s}_n\mathbf{s}_n^{\mathrm{H}} \tag{7}$$

where $\mathbf{s}_n$ contains the elements of the waveform $\mathbf{s}$ shifted by n samples and the remainder zero-filled, e.g. $\mathbf{s}_2 = [0\ \ 0\ \ s_0\cdots s_{N-3}]^{\mathrm{T}}$ and $\mathbf{s}_{-2} = [s_2\cdots s_{N-1}\ \ 0\ \ 0]^{\mathrm{T}}$.

The MMSE filter, as defined by (6) and (7), is a function of the noise covariance matrix $\mathbf{R}$, which may be known, as well as the actual range cell powers $\rho(l)$, which in practice are unknown and indicate that a unique MMSE filter must be obtained for each individual range cell. Under the assumption that the noise covariance is white, $\mathbf{R}$ can be simplified to $\sigma_v^2\mathbf{I}_N$ where σ_v^2 is the noise power and $\mathbf{I}_N$ is the $N \times N$ identity matrix. Also, while the powers of the range profile cannot be known a priori, the matched filter output as obtained in (1) can be used as an initial range profile estimate thereby enabling the computation of $\mathbf{w}(l)$ via (6) and (7), which can then be reapplied to the received signal to update the range profile estimate. Hence, the MMSE range profile estimate is obtained in bootstrapping fashion by alternating between estimating the range profile and the MMSE pulse compression filters. By simulation, it has been found that the APC algorithm needs only two to three stages of alternating estimation (after matched filtering) to suppress the range sidelobes from large target returns completely into the noise. Also, since the MMSE estimate effectively converges to the matched filter estimate when no large targets are present, the APC algorithm need only be applied in the presence of large returns which generate significant range sidelobes.

Because the original APC algorithm does not account for Doppler shift, its estimation performance is found to degrade somewhat in the presence of severe Doppler mismatch. As an example, consider a two target scenario consisting of a large scatterer with 60 dB SNR after pulse compression and a nearby smaller scatterer which would have 20 dB SNR after pulse compression were it not masked by range sidelobes from the larger scatterer. For this example, a length $N = 30$ polyphase P3 code [5] is used. The outputs of the matched filter and the original APC algorithm are shown in Fig. 1. When the Doppler mismatch for the large target is small (i.e., low target velocity and/or relatively short waveform), the mean-square error (MSE) over the $L = 100$ range cells of the processing window is -29 dB for the matched filter and -73 dB for APC. The matched

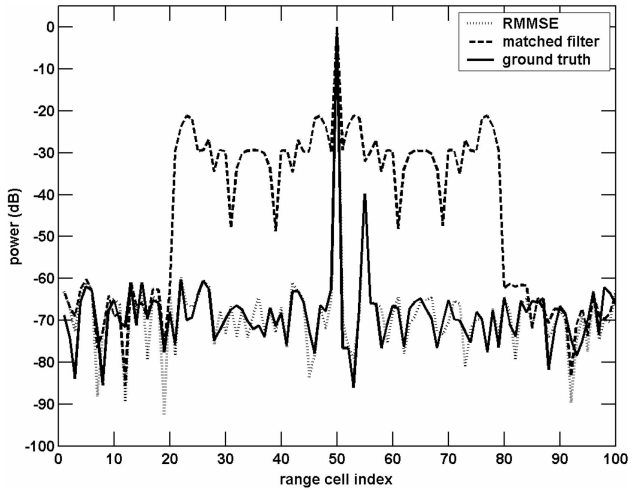

Fig. 1. Response of APC algorithm and matched filter for stationary targets.

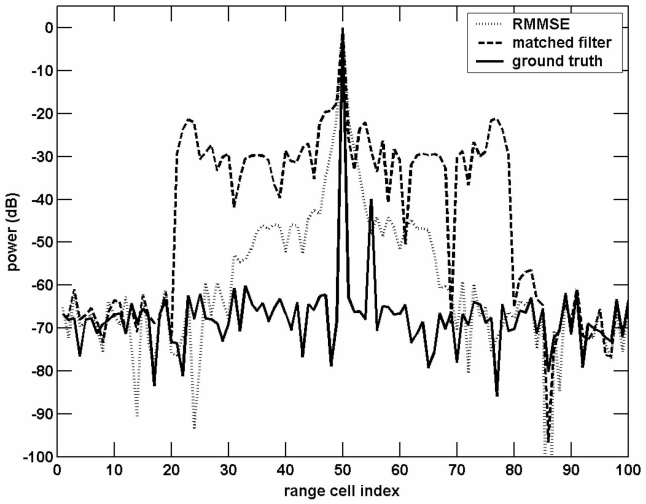

Fig. 2. Response of APC algorithm and matched filter for nonstationary target.

filter suffers from range sidelobes which mask the smaller target whereas APC suppresses the range sidelobes to the level of the noise. In contrast, Fig. 2 depicts the matched filter and APC results when very high radial velocity of the large target induces a 16° phase shift over the length of the waveform which is analogous to a Mach 2 target illuminated by a 1 μs pulse at X-band. In this case, the MSE of the matched filter is relatively unchanged at -28 dB while the MSE of the APC is now -35 dB (a 38 dB degradation over the previous example). As a result of Doppler mismatch, the performance gain of APC over the matched filter is significantly reduced. In the following section, the generalized signal model of (4) and (5) is used to incorporate the effects of Doppler into the APC formulation in order to either compensate for Doppler mismatch or enable additional discrimination capability.

III. APC WITH DOPPLER

In the presence of severe Doppler mismatch the original APC algorithm cannot completely suppress the range sidelobes resulting from large moving targets. However, two new APC-based techniques are now presented which account for the presence of Doppler. The DC-APC algorithm jointly estimates both the range profile and target Doppler in order to eliminate Doppler mismatch and thereby regain nearly all of the sidelobe suppression capability exhibited by the original APC algorithm for targets with negligible Doppler mismatch. Alternatively, the SPI technique casts the APC algorithm as an adaptive version of a bank of Doppler-shifted matched filters thus enabling some degree of range-Doppler imaging using only one pulse.

A. Doppler-Compensated APC

Using the received signal model of (4) and (5), the MMSE filter $\tilde{\mathbf{w}}(l)$ for the DC-APC algorithm is obtained by minimizing the standard MMSE cost function [13]

$$J(l) = E[|x(l) - \tilde{\mathbf{w}}^{\mathrm{H}}(l)\mathbf{y}(l)|^2] \tag{8}$$

for each individual range cell $l = 0, 1, \ldots, L-1$, where $E[\cdot]$ denotes expectation. Similar to [8], it is assumed that the range cell magnitudes are relatively stationary over the length of the waveform and that neighboring range cells are uncorrelated. The MMSE cost function in (8) is minimized by differentiating with respect to $\tilde{\mathbf{w}}^*(l)$ and setting the result equal to zero, which yields

$$\tilde{\mathbf{w}}(l) = (E[\mathbf{y}(l)\mathbf{y}^{\mathrm{H}}(l)])^{-1}E[\mathbf{y}(l)x^*(l)] \tag{9}$$

where $(\cdot)^*$ denotes complex conjugation. Substituting $\mathbf{y}(l)$ from (4), and assuming the range profile and the noise are uncorrelated, the Doppler-compensated MMSE filter is obtained as

$$\tilde{\mathbf{w}}(l) = \rho(l)(\tilde{\mathbf{C}}(l) + \mathbf{R})^{-1}\tilde{\mathbf{s}}_0(l) \tag{10}$$

where $\rho(l)$ and $\mathbf{R}$ are as previously defined, and the Doppler-compensated $N \times N$ signal correlation matrix $\tilde{\mathbf{C}}(l) = E[\tilde{\mathbf{X}}^{\mathrm{T}}(l)\mathbf{s}\mathbf{s}^{\mathrm{H}}\tilde{\mathbf{X}}^*(l)]$ can be simplified as

$$\tilde{\mathbf{C}}(l) = \sum_{n=-N+1}^{N-1} \rho(l+n)\tilde{\mathbf{s}}_n(l+n)\tilde{\mathbf{s}}_n^{\mathrm{H}}(l+n) \tag{11}$$

where $\tilde{\mathbf{s}}_n(l+n) = [0 \cdots 0 \;\; s_0 \;\; s_1 e^{j\theta_{l+n}} \cdots s_{N-n-1} \times e^{j(N-n-1)\theta_{l+n}}]^{\mathrm{T}}$ is an $N \times 1$ vector beginning with n zeros for $n > 0$, and $\tilde{\mathbf{s}}_n(l+n) = [s_{-n}e^{j(-n)\theta_{l+n}} \cdots s_{N-1} \times e^{j(N-1)\theta_{l+n}} \;\; 0 \cdots 0]^{\mathrm{T}}$ with zeros for the last $|n|$ elements for $n < 0$. As (11) illustrates, the signal correlation matrix is a function of both the range cell powers $\rho(l)$ and their respective Doppler phase shifts θ_l. Of course, as with $\rho(l)$, the Doppler phase shifts θ_l are not known a priori. Hence, an alternating estimation strategy is employed similar to that used

for the APC algorithm. Within each alternating estimation stage, the range cell powers are first estimated and then these estimated powers are used to estimate the Doppler phase shifts. Both estimates are then employed to compute the adaptive filters for the next stage. Note that the Doppler shifts are only computed for large targets as they are primarily responsible for the increase in sidelobe levels due to mismatch, as well as the fact that it is difficult to accurately estimate the Doppler shift of small targets.

For a solitary high SNR point target, the received signal of (4) can be approximately expressed as the vector

$$\mathbf{y}(l) = x(l) \cdot [s_0 \quad s_1 e^{j\theta_l} \cdots s_{N-1} e^{j(N-1)\theta_l}]^{\mathrm{T}}. \tag{12}$$

Note that for a solitary high SNR point target, all of the off-diagonal elements of $\tilde{\mathbf{X}}(l)$ (see (5)) are approximately zero. Applying the matched filter to the received signal of (12) as in (1) yields

$$\hat{x}_{\mathrm{MF}} = x(l) \cdot (|s_0|^2 + |s_1|^2 e^{j\theta_l} + \cdots + |s_{N-1}|^2 e^{j(N-1)\theta_l}). \tag{13}$$

From (13), it can be seen by inspection that, for a length-N constant modulus waveform, an estimate of the Doppler phase shift θ_l can be obtained by computing the ratio of consecutive terms in the summation. For example, the Doppler phase shift could be estimated as

$$\begin{aligned}\hat{\theta}_l &= \angle \left[\frac{x(l) \cdot (|s_1|^2 e^{j\theta_l} + \cdots + |s_{N-1}|^2 e^{j(N-1)\theta_l})}{x(l) \cdot (|s_0|^2 + \cdots + |s_{N-2}|^2 e^{j(N-2)\theta_l})} \right] \\ &= \angle \left[e^{j\theta_l} \frac{(1 + e^{j\theta_l} + \cdots + e^{j(N-2)\theta_l})}{(1 + e^{j\theta_l} + \cdots + e^{j(N-2)\theta_l})} \right] \end{aligned} \tag{14}$$

where $\angle[\cdot]$ is the phase angle of the complex argument and the constant modulus assumption of $|s_0|^2 = |s_1|^2 = \cdots = |s_{N-1}|^2$ has been applied. The denominator in (14) is the first $N-1$ elements in the summation of (13), and the numerator is the last $N-1$ elements in the summation. The partial summations in (14) can be obtained through the application of portions of the matched filter (i.e., the first $N-1$ elements of the matched filter and the last $N-1$ elements of the matched filter, respectively, for the above example).

In general, the partial matched filters can be applied as

$$\mathbf{g}(l) = \mathbf{B}_{\mathrm{MF}}^{\mathrm{H}} \mathbf{y}(l) \tag{15}$$

where

$$\mathbf{B}_{\mathrm{MF}} = \begin{bmatrix} \bar{\mathbf{s}}_0 & & & 0 \\ & \bar{\mathbf{s}}_1 & & \\ & & \ddots & \\ 0 & & & \bar{\mathbf{s}}_M \end{bmatrix}_{N \times (M+1)}. \tag{16}$$

$M \in [1, 2, \ldots, N-1]$ is the number of partial matched filters, and the $N-M$ length vector $\bar{\mathbf{s}}_m = [s_m \cdots s_{N-M+m-1}]^{\mathrm{T}}$, $m = 0, 1, \ldots, M$, is the mth partial matched filter. In much the same manner as (15), the $M+1$ elements of the vector $\mathbf{g}(l)$ can be used to estimate the Doppler phase shift θ_l as either

$$\hat{\theta}_l = \angle \left[\sum_{m=1}^{M} \frac{g_m(l)}{g_{m-1}(l)} \right] \tag{17}$$

or as

$$\hat{\theta}_l = \frac{1}{M} \sum_{m=1}^{M} \angle \left[\frac{g_m(l)}{g_{m-1}(l)} \right] \tag{18}$$

where $g_m(l)$ is the mth element of $\mathbf{g}(l)$. The estimate of (17) will be heavily influenced by dominant values of the quotient resulting from outlier terms in $\mathbf{g}(l)$ (although it can reasonably be expected that all terms will be of comparable magnitude). Conversely, the estimate in (18) is unaffected by magnitude variations but may be more sensitive to phase errors. By varying the value of M, a trade-off exists between near full pulse compression integration gain ($M = 1$) and the maximum number of samples over which to average the Doppler phase shift estimate ($M = N-1$). It has been determined through simulation that values approximately half-way between these two extremes (i.e., $M \approx N/2$) tend to provide the most accurate estimate of the Doppler phase shift.

Although estimation of the Doppler phase shift via matched filtering is computationally efficient, the performance is satisfactory only in cases where solitary point targets are present (i.e., targets sparsely populated in range). The matched filter based estimate degrades when one or more targets with comparable SNR are in relatively close proximity. To mitigate the effects of interference from other nearby targets (i.e., range sidelobes) on the estimation of $\hat{\theta}_l$, the phase estimation scheme described above can also use subfilter versions of the (non-Doppler-compensated) adaptive MMSE filter (6) by replacing $\mathbf{B}_{\mathrm{MF}}$ in (16) with

$$\mathbf{B}_{\mathrm{MMSE}}(l) = \begin{bmatrix} \bar{\mathbf{w}}_{\mathbf{0}}(l) & & & 0 \\ & \bar{\mathbf{w}}_1(l) & & \\ & & \ddots & \\ 0 & & & \bar{\mathbf{w}}_M(l) \end{bmatrix}_{N \times (M+1)}. \tag{19}$$

The length $N-M$ vector $\bar{\mathbf{w}}_m(l)$ is the mth MMSE subfilter, and is computed by partitioning (6) and (7) as

$$\bar{\mathbf{w}}_m(l) = \rho(l)(\bar{\mathbf{C}}_m + \bar{\mathbf{R}})^{-1} \bar{\mathbf{s}}_m \tag{20}$$

where $\bar{\mathbf{R}}$ is an $(N-M) \times (N-M)$ principal submatrix [17] of contiguous rows and columns of the Toeplitz temporal noise covariance matrix $\mathbf{R}$ and the $(N-M) \times$

$(N-M)$ matrix $\bar{\mathbf{C}}_m(l)$ is the $(m+1)$st principal submatrix of contiguous rows and columns of $\mathbf{C}(l)$ from (7) for $m = 0,\ldots,M$. In order to minimize the likelihood of mis-estimating θ_l, only the Doppler shifts of relatively large target returns are estimated, reducing the possibility of the estimate of θ_l for small targets being skewed by nearby large targets. A variable threshold can be set according to the noise power and/or current local power estimates in order to determine which range cells are candidates for Doppler estimation. With each successive stage, as the range sidelobes are decreased the threshold can be reduced accordingly, allowing the Doppler phase of the lesser large targets to be estimated. In addition, as a robustness measure an upper limit may be placed on the value of the Doppler estimate such that it is maintained within practical bounds for the specific radar application and scenario.

The Doppler phase shift estimate obtained from either (17) or (18) is incorporated into the Doppler-compensated MMSE filter formulation of (10) and (11) along with the current range cell power estimates in order to re-estimate the appropriate adaptive receive filter for each individual range cell. As with the original APC algorithm, it has been found via simulation that 2–3 stages (excluding initial matched filtering) enable DC-APC to almost completely remove Doppler-mismatch-induced range sidelobes.

B. Single Pulse Imaging

Instead of compensating for the effects of Doppler mismatch as done by the DC-APC algorithm, the SPI algorithm exploits Doppler in a manner somewhat similar to inverse synthetic aperture radar (ISAR), which may operate on hundreds to thousands of pulses. In contrast, SPI produces a range-Doppler image from the returns from a single pulse. Of course, the short temporal baseline of a single pulse imposes a fundamental limit in terms of Doppler resolution and thereby makes SPI applicable primarily for targets at rather high velocities or exhibiting high maneuverability. However, the benefit of the short temporal baseline is that nonlinear motion (e.g. acceleration and/or range walking) is essentially negligible thus potentially enabling SPI to be of use for automatic target recognition (ATR).

The SPI technique is effectively the adaptive version of a bank of Doppler-shifted matched filters and is based upon a multistatic implementation of the APC algorithm denoted as MAPC [14–16] which jointly separates and pulse compresses multiple concurrently received signals resulting from illumination by multiple different waveforms. For the SPI algorithm, which is applied to a monostatic radar return signal, the multiple different waveforms are Doppler-shifted versions of the same transmitted waveform.

Consider a simplistic scenario in which all scatterers are moving at the same velocity r relative to the radar platform. The motion relative to the radar platform induces a Doppler phase shift θ between samples in the received signal from each scatterer. The length-N vector $\mathbf{s}$ denotes the discrete-time version of the transmitted waveform and the length-N vector $\mathbf{x}(l,\theta) = [x(l,\theta)\ \ x(l-1,\theta)\cdots x(l-N+1,\theta)]^{\mathrm{T}}$ represents a set of N contiguous samples of the range profile impulse response. Note that here the range profile is a function of θ, highlighting the fact that all of the scatterers in the range profile are moving at the same relative velocity and therefore induce the same per-sample Doppler phase shift θ in the radar return signal. The lth sample of the received radar return as a function of θ is defined as

$$y(l,\theta) = (\mathbf{x}(l,\theta) \circ \mathbf{d}(\theta))^{\mathrm{T}}\mathbf{s} + v(l) \tag{21}$$

for, $l = 0,\ldots,L+N-2$. The N-dimensional vector $\mathbf{d}(\theta) = [1\ \ e^{j\theta}\ \ e^{j2\theta}\cdots e^{j(N-1)\theta}]^{\mathrm{T}}$ contains the relative phase shifts of the N contiguous samples of $\mathbf{x}(l,\theta)$ where θ is the Doppler phase shift between successive received samples. Note that $\mathbf{d}(\theta)$ is a different representation of the Doppler phase shifts than was $\mathbf{e}(\theta)$ in the previous section.

Although the received radar return signal model of (21) is for scatterers moving at the same relative velocity, the model can easily be generalized to include scatterers moving at all possible velocities by integrating the received signal portion of (21) over every possible Doppler phase shift (note that integration here represents the inclusion of received signal components over all values of θ and hence is not performed on the noise term). The lth sample of the total received signal is then

$$y(l) = \int_{-\pi}^{\pi} (\mathbf{x}(l,\theta) \circ \mathbf{d}(\theta))^{\mathrm{T}}\mathbf{s}\,d\theta + v(l). \tag{22}$$

Approximating the integration over θ in (23) with a summation over K values of θ then yields

$$y(l) = \sum_{k=1}^{K} (\mathbf{x}(l,\theta_k) \circ \mathbf{d}(\theta_k))^{\mathrm{T}}\mathbf{s} + v(l) \tag{23}$$

where

$$\theta_k = -\pi + \frac{2\pi}{K-1}(k-1), \qquad k = 1,\ldots,K \tag{24}$$

and K is arbitrarily large, such that (23) is a good approximation of (22). For notational simplicity, we shall henceforth denote $\mathbf{x}(l,\theta_k) \triangleq \mathbf{x}_k(l)$. By rearranging terms, (23) can be expressed as

$$y(l) = \sum_{k=1}^{K} \mathbf{x}_k^{\mathrm{T}}(l)\tilde{\mathbf{s}}_k + v(l) \tag{25}$$

where

$$\tilde{\mathbf{s}}_k = \mathbf{s} \circ \mathbf{d}(\theta_k) \tag{26}$$

is a Doppler phase-shifted version of the transmitted waveform. The collection of N samples of the received return signal $\mathbf{y}(l) = [y(l)\ \ y(l+1)\cdots y(l+N-1)]^{\mathrm{T}}$ can therefore be expressed as

$$\mathbf{y}(l) = \sum_{k=1}^{K} \mathbf{X}_k^{\mathrm{T}}(l)\tilde{\mathbf{s}}_k + \mathbf{v}(l) \tag{27}$$

where

$$\begin{aligned}\mathbf{X}_k(l) &= [\mathbf{x}_k(l)\mathbf{x}_k(l+1)\cdots\mathbf{x}_k(l+N-1)] \\ &= \begin{bmatrix} x_k(l) & x_k(l+1) & \cdots & x_k(l+N-1) \\ x_k(l-1) & x_k(l) & & x_k(l+N-2) \\ \vdots & \vdots & \ddots & \vdots \\ x_k(l-N+1) & x_k(l-N+2) & \cdots & x_k(l) \end{bmatrix}.\end{aligned} \tag{28}$$

As shown by (27), a radar return from multiple targets with varying velocities can be represented as a summation of the returns from K distinct range profiles, each illuminated by a different waveform $\tilde{\mathbf{s}}_k$. Essentially, by moving the Hadamard product with the Doppler phase shift vector $\mathbf{d}(\theta)$ from the range profile to the waveform, the signal model has been transformed from a single system that is not linear time invariant (LTI), due to the range profile phase dependence on Doppler, to a summation of K distinct LTI systems. In so doing, the radar return signal model given by (27) is now mathematically identical to that used for the derivation of the MAPC algorithm [14–16]. Hence, using the MAPC formulation and solution, the SPI algorithm is able to accurately estimate the range profile associated with each Doppler thereby producing an estimate of the two-dimensional range-Doppler image.

Doppler-shifted versions of the transmitted waveform in the signal model of (27) are exactly the same as that employed by a standard bank of Doppler-shifted matched filters which partitions the Doppler space such that at least one of the filters will closely match a particular moving target and thus realize close to full coherent integration gain. In order to facilitate the greatest Doppler resolution, a waveform with a thumbtack-type ambiguity function is most applicable. Because the peak for the thumbtack waveform ambiguity function is narrow in both range and Doppler, the range/Doppler "location" of a given target can be more accurately determined than would be possible for a Doppler-tolerant waveform such as linear frequency modulation (LFM).

Were one to use the standard bank of Doppler-shifted matched filters, the lth range cell for the kth Doppler shift could be estimated as

$$\hat{x}_{\mathrm{MF},k}(l) = \tilde{\mathbf{s}}_k^{\mathrm{H}}\mathbf{y}(l) \tag{29}$$

for $k = 1,2,\ldots,K$ where $\hat{x}_{\mathrm{MF},k}(l)$ is a range profile estimate associated with a Doppler-shifted version of the matched filter; $\hat{x}_{\mathrm{MF},k}(l)$ can thus be considered a "Doppler range profile." However, as with a single matched filter, the bank of Doppler-shifted matched filters has a limited sensitivity in the neighborhood of large return signals due to range and Doppler sidelobes. To ameliorate the sidelobe effects of traditional matched filtering, the bank of matched filters $\mathbf{s}_k$ in (29) is replaced by a bank of MMSE-based adaptive filters. The MMSE cost function [6] is minimized for each range cell associated with each Doppler range profile as

$$J_k(l) = E[|x_k(l) - \mathbf{w}_k^{\mathrm{H}}(l)\mathbf{y}(l)|^2] \tag{30}$$

where $\mathbf{w}_k(l)$ is the MMSE weight vector for the lth range cell for the range profile associated with Doppler phase shift θ_k. The solution to (30) takes the form [14–16]

$$\mathbf{w}_k(l) = \hat{\rho}_k(l)\left(\sum_{i=1}^{K}\mathbf{C}_i(l) + \mathbf{R}\right)^{-1}\tilde{\mathbf{s}}_k \tag{31}$$

where $\hat{\rho}_k(l) = |\hat{x}_k(l)|^2$ is the estimated power of $x_k(l)$, $\mathbf{R} = E[\mathbf{v}(l)\ \ \mathbf{v}(l)^{\mathrm{H}}]$ is the noise covariance matrix, and the ith signal correlation matrix is given by

$$\mathbf{C}_i(l) = \sum_{n=-N+1}^{N-1}\hat{\rho}_k(l+n)\tilde{\mathbf{s}}_{i,n}\tilde{\mathbf{s}}_{i,n}^{\mathrm{H}} \tag{32}$$

where $\tilde{\mathbf{s}}_{i,n}$ contains the elements of the Doppler phase-shifted waveform $\tilde{\mathbf{s}}_i$ shifted by n samples and zero-filled in the remaining n samples, e.g. $\tilde{\mathbf{s}}_{i,2} = [0\ \ 0\ \ \tilde{s}_i(0)\cdots\tilde{s}_i(N-3)]^{\mathrm{T}}$ and $\tilde{\mathbf{s}}_{i,-2} = [\tilde{s}_i(2)\cdots\tilde{s}_i(N-1)\ \ 0\ \ 0]^{\mathrm{T}}$.

As seen from (31) and (32), initial estimates of the K Doppler-shifted range profiles, as well as the noise covariance matrix $\mathbf{R}$, are required to form the weight vectors $\mathbf{w}_k$. Assuming the noise covariance is white Gaussian, $\mathbf{R}$ may be simplified to $\sigma_v^2\mathbf{I}_N$, where σ_v^2 is the noise power, and $\mathbf{I}_N$ is the $N \times N$ identity matrix. Similar to that previously discussed for the APC algorithm, initial range profile estimates can be obtained by first applying the standard bank of Doppler-shifted matched filters. In bootstrapping fashion the MMSE range profile estimates are then obtained by alternating between updating the MMSE filters of (31) and updating the K sets of range profile estimates. It has been found via simulation that 4–6 stages of alternating estimation are needed to achieve good sidelobe suppression. Furthermore, the structure of the MMSE estimator in (31) enables fast implementation via Woodbury's identity (i.e., the matrix inversion lemma) [18] through a straightforward extension of the approach used in [13].

To discuss Doppler resolution we first introduce the term $\phi = 2\pi fT$ which is the total Doppler phase

shift (in radians) induced by Doppler frequency f over the (temporal) length of the waveform T (as opposed to the phase shift between successive received samples previously specified as θ). We cast Doppler resolution in terms of the phase deviation over the pulse because this framework is then generalized for any pulse length or Doppler frequency (and by direct extension any operating frequency). It is well known from ambiguity analysis based on matched filter processing (see [1, pp. 332–338]) that the Doppler resolution of a single thumbtack-like pulse is $\Delta f = 1/T$. Thus in terms of phase over the pulse length, the Doppler-shifted bank of matched filters possesses a Doppler resolution of $\Delta\phi = 2\pi\Delta fT = 2\pi$. In contrast, because SPI is adaptive for each Doppler-shifted range cell, a meaningful metric of Doppler resolution is not available. However, based on the "rule-of-thumb" that two equal-power scatterers are nominally separable if there exists a -3 dB null between them, it has been found empirically via simulation that the SPI algorithm can resolve them when the phase difference is $\Delta\phi \geq \pi$.

However, the trade-off for achieving this improved Doppler resolution as well as the suppression of range and Doppler sidelobes is that the approximation in (23) requires K to be sufficiently large to accurately represent the possible Doppler shifts present (i.e., oversampling in Doppler). Experimentation via simulation has shown that specifying the Doppler partitioning for SPI such that contiguous Doppler-shifted versions of the transmit waveform have total phase-shift differences of $\Delta\phi \leq \pi/5$ provides a sufficiently dense representation in the Doppler domain. The need for Doppler oversampling is a result of Doppler mismatch effects which, as discussed previously, fundamentally limit the suppression of sidelobes. Note, though, that large values of ϕ need not be included (relative to the particular application) as these may represent Doppler shifts which would not be expected to occur in practice.

IV. SIMULATION RESULTS

The performance potential of the two new APC-based techniques is now illustrated through simulation examples with targets exhibiting significant Doppler with respect to the radar platform. It is shown that the DC-APC algorithm and the SPI technique are both dramatically superior to standard matched filtering approaches because they both estimate range and Doppler parameters of the illuminated range profile adaptively.

A. Doppler-Compensated APC

The performance of the DC-APC algorithm is demonstrated by comparing its performance with that of the matched filter and the original APC algorithm for three simulated scenarios. The first case consists of a large scatterer with significant Doppler shift near a small stationary scatterer that is masked by range sidelobes. The second case consists of several approaching and receding large targets interspersed with small stationary targets. The final case is the most stressing with both large and small targets distributed randomly in range with potentially large random Doppler shifts. In all three cases, the performance of the DC-APC algorithm outperforms both the matched filter and the original APC algorithm. The performance of each algorithm is assessed by measuring the MSE between the range profile ground truth and the respective range profile estimates.

The waveform employed for all three cases is the length $N = 30$ polyphase Lewis-Kretschmer P3 code [5], which upon receive (after down-conversion to baseband) is defined as

$$s(n) = e^{j(\pi/N)n^2}, \qquad n = 0, 1, \ldots, N-1. \tag{33}$$

While DC-APC and APC are both waveform independent [13], the DC-APC algorithm has been found to perform better for Doppler-tolerant waveforms, such as the P3 code, because the Doppler-tolerant nature ensures sufficient SNR for accurate Doppler phase-shift estimation. For all three cases, the ground truth radar range profiles consist of point scatterer targets in noise which is modeled as zero-mean complex Gaussian. For the purpose of estimating Doppler phase shift by the DC-APC algorithm, the parameter M is set as $M = N/2 = 15$, and (17) is used. The APC and DC-APC algorithms employ 3 stages of alternating estimation (following initial matched filter estimation) for all three cases.

For the first case, the scenario is the same as that presented in the example at the end of Section II (Figs. 1 and 2). A large moving scatterer and a small stationary scatterer are placed in close proximity to one another with the power of the small scatterer 40 dB lower than that of the larger scatterer which itself has an SNR of 60 dB. Also, the large scatterer has a Doppler shift of 16° over the length of the waveform which is analogous to a Mach 2 target illuminated by a 1 μs pulse from an X-band radar. The results from this case are illustrated in Fig. 3 where, as expected, large range-induced sidelobes are present in the output of the matched filter thus masking the small target. The APC algorithm suffers from Doppler-mismatch-induced range sidelobes also resulting in the masking of the small target. However, by estimating and then compensating for the Doppler mismatch, the DC-APC algorithm is able to estimate the range profile nearly to the level of the noise. In terms of MSE performance, the matched filter, APC algorithm, and DC-APC

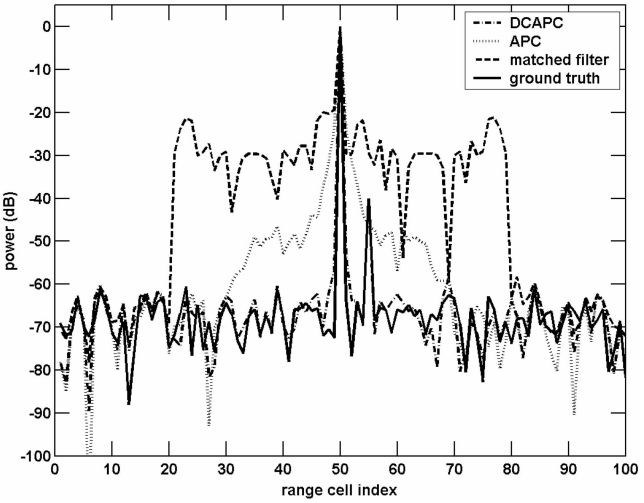

Fig. 3. Response of algorithms for nonstationary target. DCAPC algorithm suppresses sidelobes into noise, unmasking small target.

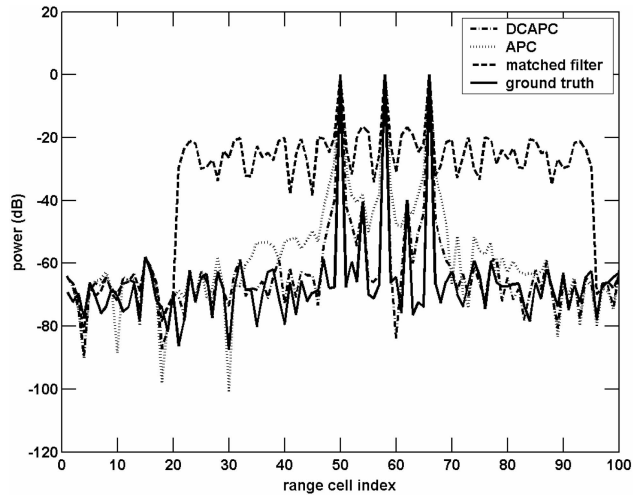

Fig. 4. Response of algorithms for multiple nonstationary targets. Small targets masked by APC but detectable with DCAPC.

algorithm achieve −28 dB, −35 dB, and −59 dB, respectively.

The second target scenario contains five targets: three large moving targets interspersed with two smaller stationary targets. As in the previous example, the power of the smaller targets is 40 dB below that of the larger targets which all have an SNR of 60 dB. The three large targets have Doppler shifts of +15°, −5°, and +10° over the length of the waveform, respectively. Hence, the three targets are moving at significantly different velocities with the 1st and 3rd approaching the radar platform and the 2nd receding. The results are shown in Fig. 4 in which the matched filter performs poorly. The APC algorithm outperforms the matched filter, yet its estimation performance is again degraded due to Doppler mismatch. The effects of Doppler mismatch are significantly suppressed by the DC-APC algorithm, resulting in the unmasking of the two small stationary

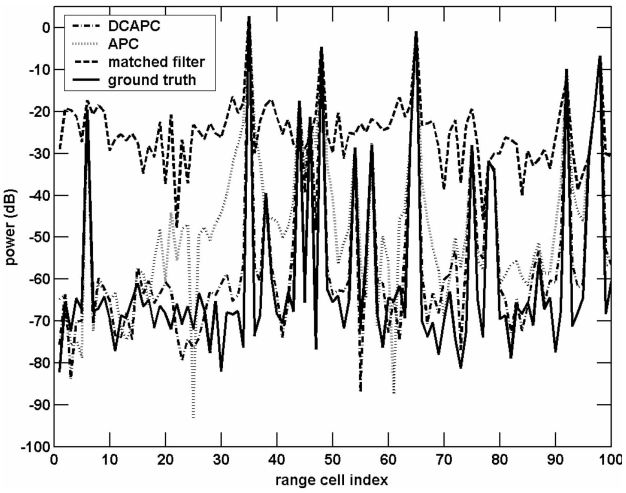

Fig. 5. Response of algorithms for dense nonstationary target scenario.

targets. The matched filter, APC, and DC-APC approaches achieve MSE levels of −24 dB, −35 dB, and −59 dB, respectively.

The final case is a scenario containing numerous targets randomly distributed in range with greatly varying powers and randomly assigned Doppler shifts. The targets possess Doppler shifts that are at most ±25° over the length of the waveform. Fig. 5 illustrates the result from applying the three techniques. The matched filter exhibits the usual range sidelobes masking the smaller targets and yielding an MSE of −23 dB. The performance of the APC algorithm is significantly better than that of the matched filter with −36 dB MSE yet some of the smaller targets are masked due to the effects of Doppler mismatch on the larger targets. By comparison, the DC-APC algorithm more effectively suppresses the sidelobes thereby unmasking nearly all of the small targets with a resulting MSE of −48 dB.

B. Single Pulse Imaging

The performance of the SPI algorithm is assessed by comparison with a bank of Doppler-shifted matched filters for two simulated target scenarios. The first case involves a large scatterer surrounded by four small scatterers, two of which occupy the same range cell as the large scatterer but with substantially different Dopplers (for example, the blades of a helicopter). To demonstrate Doppler resolution, the second case consists of two equal-size scatterers at the same range cell with nominally different Doppler shifts. For both cases, the transmit waveform is an $N = 30$ random polyphase waveform. To provide additional robustness for the SPI algorithm the adaptive filter for each range and Doppler is normalized by $1/(\mathbf{w}_k^{\mathrm{H}}(l)\tilde{\mathbf{s}}_k)$ so that $\mathbf{w}_k^{\mathrm{H}}(l)\tilde{\mathbf{s}}_k = 1$. Also, the imaging results shown for both the matched filter bank and SPI are lower-bounded at

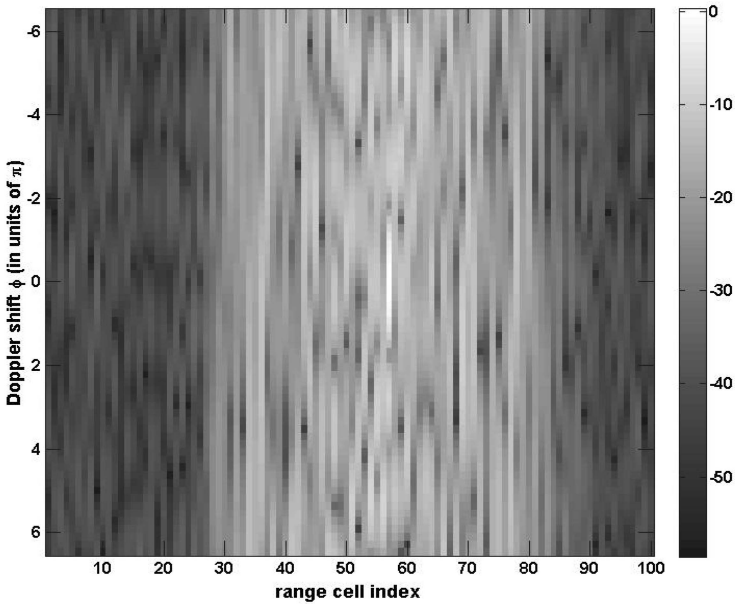

Fig. 6. Response of matched filter bank. Due to sidelobes, large target spreads in range and Doppler.

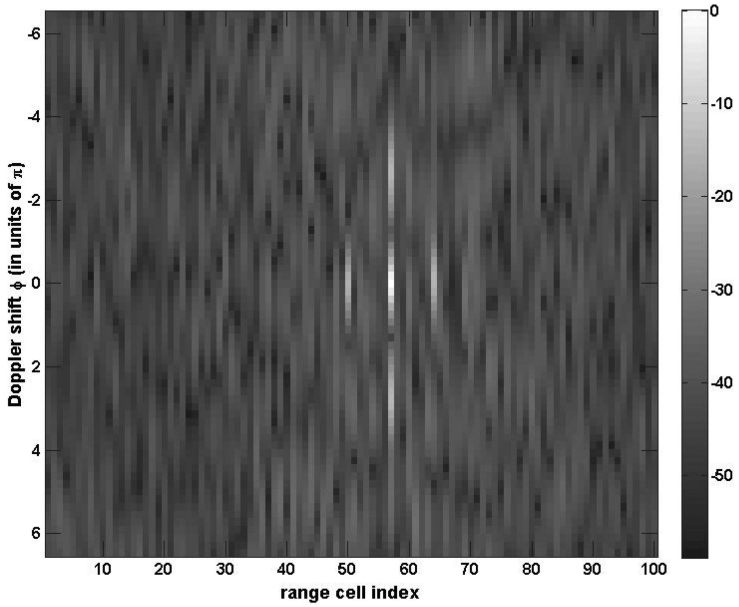

Fig. 7. Response of SPI algorithm. All five scatterers easily visible.

the after-processing noise floor σ_v^2/N to provide better visualization over the high dynamic range.

For the first case, the large stationary scatter has an SNR of 30 dB (before pulse compression) with the other four scatterers 15 dB lower. Two of the small scatterers are stationary, located 7 range cells before and after the large scatterer. The other two small scatterers are in the same range cell as the large scatterer, but possess Doppler phase shifts over the length of the waveform of $\phi = \pm 2.75\pi$ (analogous to a Mach 2 scatterer illuminated by a 3.5 μs pulse at W-band). The resulting images from applying a bank of Doppler-shifted matched filters and after five stages of the SPI algorithm are shown in Figs. 6 and 7, respectively. For the bank of matched filters, the large scatterer dominates the image and completely masks the presence of the other scatterers. However, all of the scatterers are easily identifiable in the SPI image in which the range and Doppler sidelobes have been suppressed into the noise.

For the second case, two large scatterers (60 dB before pulse compression) are present at the same range cell with equal return signal power but with differing Doppler shifts. One of the scatterers is stationary and the other has a Doppler shift over the length of the waveform of $\phi = \pi$, the experimentally-determined (via simulation) limit for which SPI can resolve two scatterers in Doppler. The

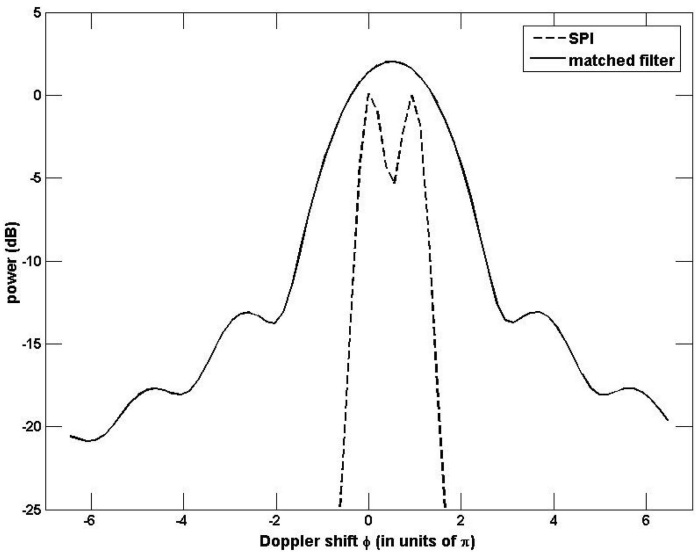

Fig. 8. Resolving two scatterers in same range cell with Doppler phase shift difference of $\Delta\phi = \pi$ over length of pulse.

outputs of the matched filter bank and four stages of SPI are depicted in Fig. 8, in which a cross section in Doppler is shown for the range cell containing the two scatterers. While the two scatterers appear as one in the output of the matched filter bank, they are clearly distinguishable in the output of the SPI algorithm.

V. CONCLUSIONS

While still superior to deterministic matched/mismatched filtering techniques, the performance gain of the APC algorithm is known to be limited when applied to radar return signals possessing severe Doppler mismatch. To ameliorate the effects of Doppler mismatch over a single pulse, two Doppler-sensitive variations of APC have been introduced. The DC-APC algorithm jointly estimates both the illuminated range profile and the Doppler phase shifts of large targets. The Doppler estimates are incorporated into the APC adaptive receive filter formulation in order to compensate for Doppler mismatch and thereby regain nearly all of the sensitivity improvement of APC. In contrast, the SPI algorithm generalizes the APC formulation for a bank of Doppler-shifted matched filters to enable range/Doppler sidelobe suppression and thereby provides range-Doppler imaging capability of the return signal of a single radar pulse. As such, the SPI algorithm is applicable to targets comprised of scatterers with substantial variation in Doppler (such as helicopter blades). Current and future work is focused on extending the temporal baseline of the SPI algorithm to accommodate additional pulses (albeit still much less than that required for ISAR) in order to greatly improve the Doppler resolution.

REFERENCES

[1] Skolnik, M. I.
Introduction to Radar Systems (3rd ed.).
New York: McGraw-Hill, 2001, 332–369.

[2] Ackroyd, M. H., and Ghani, F.
Optimum mismatched filter for sidelobe suppression.
IEEE Transactions on Aerospace and Electronic Systems, **AES-9** (Mar. 1973), 214–218.

[3] Felhauer, T.
Digital signal processing for optimum wideband channel estimation in the presence of noise.
IEE Proceedings, Pt. F, **140**, 3 (June 1993), 179–186.

[4] Song, S. M., Kim, W. M., Park, D., and Kim, Y.
Estimation theoretic approach for radar pulse compression processing and its optimal codes.
Electronic Letters, **36**, 3 (Feb. 2000), 250–252.

[5] Lewis, B. L., and Kretschmer, F. F.
Linear frequency modulation derived polyphase pulse compression codes.
IEEE Transactions Aerospace and Electronic Systems, **AES-18**, 5 (Sept. 1982), 637–641.

[6] Kretschmer, F. F., Jr., and Gerlach, K.
Low sidelobe radar waveforms derived from orthogonal matrices.
IEEE Transactions on Aerospace and Electronic Systems, **27**, 1 (Jan. 1991), 92–102.

[7] Altes, R.
Optimum waveforms for sonar velocity discrimination.
Proceedings of the IEEE, **59**, 11 (Nov. 1971), 1615–1617.

[8] Nathanson, F. E., Reilly, J. P., and Cohen, M. N.
Radar Design Principles (2nd ed.).
Raleigh, NC: SciTech Publishing, 1999, 362–363.

[9] Zeng, Y., Lin, Z., Bi, G., Yeo, J., and Lu,,S.
Dilation dependent matched filtering for SAR signal processing.
IEEE Transactions on Aerospace and Electronic Systems, **41**, 2 (Apr. 2005), 729–736.

[10] Kay, S. M.
Fundamentals of Statistical Signal Processing: Estimation Theory.
Upper Saddle River, NJ: Prentice-Hall, 1993, 219–286, 344–350.

[11] Blunt, S. D., and Gerlach, K.
A novel pulse compression scheme based on minimum mean-square error reiteration.
In *Proceedings of the IEEE International Radar Conference*, Sept. 3–5, 2003, 349–353.

[12] Blunt, S. D., and Gerlach, K.
Adaptive pulse compression.
In *Proceedings of the IEEE National Radar Conference*, Apr. 26–29, 2004, 271–276.

[13] Blunt, S. D., and Gerlach, K.
Adaptive pulse compression via MMSE estimation.
IEEE Transactions on Aerospace and Electronic Systems, **42**, 2 (Apr. 2006), 572–584.

[14] Blunt, S. D., and Gerlach, K.
Joint adaptive pulse compression to enable multistatic radar.
Presented at the IEE Waveform Diversity and Design Conference, Edinburgh, Scotland, Nov. 8–10, 2004.

[15] Blunt, S. D., and Gerlach, K.
Aspects of multistatic adaptive pulse compression.
In *Proceedings of the IEEE International Radar Conference*, Arlington, VA, May 9–12, 2005, 104–108.

[16] Blunt, S. D., and Gerlach, K.
Multistatic adaptive pulse compression.
IEEE Transactions on Aerospace and Electronic Systems, **42**, 3 (2006), 891–903.

[17] Horn, R. A., and Johnson, C. R.
Matrix Analysis.
New York: Cambridge University Press, 1985, 17.

[18] Moon, T. K., and Stirling, W. C.
Mathematical Methods and Algorithms for Signal Processing.
Upper Saddle River, NJ: Prentice-Hall, 2000, 258.

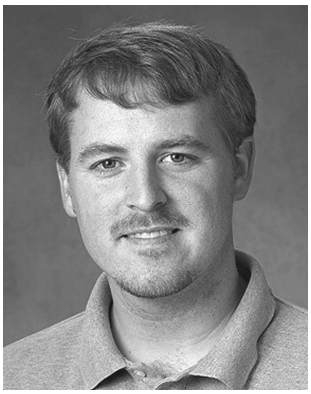

Shannon D. Blunt (S'96—M'02—SM'07) received the B.S., M.S., and Ph.D. degrees in electrical engineering in 1999, 2000, and 2002, respectively, from the University of Missouri, Columbia.

From 2002 to 2005 he was with the Radar Division of the Naval Research Laboratory in Washington, D.C. Since 2005 he has been with the Department of Electrical Engineering and Computer Science at the University of Kansas where he is affiliated with the Radar Systems & Remote Sensing Lab (RSL). His research interests are in signal processing and system design for radar, communications, and biomedical imaging with a particular emphasis on waveform diversity techniques.

Dr. Blunt received the Air Force Office of Scientific Research (AFOSR) Young Investigator Award in 2007. He is presently serving as an associate editor for *IEEE Transactions on Aerospace and Electronic Systems* (AESS), is a member of the IEEE AESS Radar Systems Panel, and is cochairing the 2009 International Waveform Diversity & Design Conference. He is also a member of Eta Kappa Nu and Tau Beta Pi and serves as a faculty advisor to the Kansas Alpha chapter of Tau Beta Pi.

Aaron K. Shackelford (S'97—M'04) was born in Kansas City, MO. He received the B.S., M.S., and Ph.D. degrees in electrical engineering in 1999, 2001, and 2004, respectively, from the University of Missouri, Columbia.

Since 2004, he has been employed by the Radar Division of the Naval Research Laboratory in Washington, D.C. His research interests include adaptive signal processing, waveform diversity techniques, pattern recognition, and remote sensing.

Dr. Shackelford received the NRL Alan Berman Research Publication Award in 2007. He was a recipient of the NASA Graduate Student Researchers Program Fellowship and is a member of Tau Beta Pi.

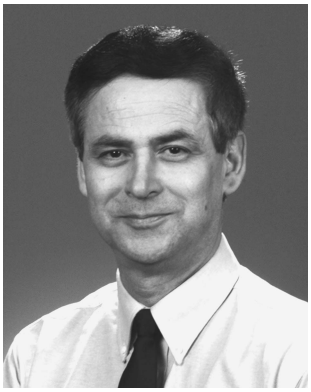

Karl Gerlach (M'81—F'02) received a B.S. degree in 1972 from the University of Illinois, Urbana, and M.S. and D.Sc. degrees from George Washington University, Washington, D.C., in 1975 and 1981, respectively, all in electrical engineering.

Since 1972, he has been employed by the Naval Research laboratory, Washington, D.C. From 1972–1976, he worked on experimental submarine communications systems, and from 1976 to the present, he has been with the Radar Division, where his research interests include adaptive signal processing, space-based radar, and ultrawideband radar.

Dr. Gerlach was the 1986 recipient of the IEEE AESS Radar Systems Panel Award and the 2002 IEEE AES M. Barry Carlton award.

Kevin Smith Biography and photo not available.